Draft version September 15, 2022
Typeset using LaTeX **modern** style in AASTeX61

MAPPING NEUTRAL CARBON ACROSS THE OUTER LAYERS OF THE HELIX NEBULA WITH THE ATACAMA COMPACT ARRAY

Lucille Steffes[1,2] and Jesse Bublitz[2]

[1] *University of Wisconsin–Madison, Department of Astronomy, 475 N Charter St, Madison, WI 53703, USA*
[2] *Green Bank Observatory, 155 Observatory Road, Green Bank, WV 24944, USA*

ABSTRACT

The Atacama Compact Array (ACA) was used to map and examine the abundance of neutral atomic carbon [C I] at three regions in the outer layers of the Helix Nebula (NGC 7293). Strong detections of [C I] were found and subsequently mapped for two of the regions, the Rim and East Positions. However, due to low integration times, a detection of [C I] was not resolved at the West Position, so upper limits were calculated instead. Globule-like structures, which had previously been obscured by dust, were also observed at the Rim Position at two different velocities, giving more information about the barrel structure of the Helix Nebula. Maps of [C I] were also compared to high energy transitions from the Hubble Space Telescope and to IRAM-30m single dish molecular observations in the same regions.

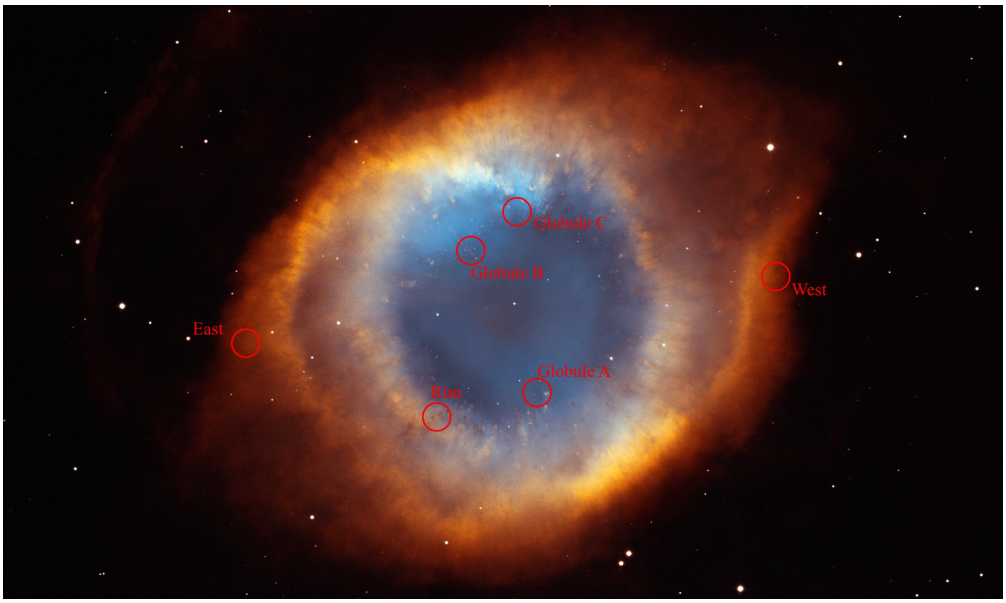

Figure 1. Optical composite image of the Helix Nebula. Credit: NASA, NOAO, ESA, the Hubble Helix Nebula Team, M. Meixner (STScI), and T.A. Rector (NRAO)

1. INTRODUCTION

The Helix Nebula (NGC 7293) represents the nearest known planetary nebula (200±1 pc Gaia Collaboration et al. 2018). A planetary nebula (PN) consists of the outer remnants of a dying low mass star, which is on its way to becoming a white dwarf. During the end of the Asymptotic Giant Branch (AGB) phase, the outer layers of the star are ejected, leaving behind the central star of the planetary nebula (CSPN). This CSPN emits high intensity ultraviolet radiation, creating an ionized cavity around the CSPN and driving the photo-dissociation region (PDR) chemistry on the edge of the cavity. Like other, much larger PDRs, the rings of the Helix Nebula are rich in molecules (Bublitz, Steffes, et al, 2022, in prep). Important aspects to the PDR have been mapped in detail before, such as H_2, molecules in the cold dense regions, and ionized elements such as [O III] and $H\alpha$. There has not been a high resolution map of the important intermediary atomic neutral carbon ([C I]) gas across the Helix Nebula since 1997 and only a 6×8 square arcmin region in near the West Position mapped in 2014 (with spatial resolutions of 15″ and 30″ respectively; Young et al. 1997; Etxaluze, M. et al. 2014).

As an intermediary between ionized and molecular gas, [C I] facilitates the transition between the ionized gas in the ionized cavity and the molecular gas in denser regions further from the CSPN. As the gas is irradiated, molecular bonds are broken, which can leave individual carbon atoms that either aid in shielding from irradiation or form new bonds with other atoms. While the Helix Nebula has been found to be oxygen rich, there is still an abundance of carbon-bearing molecules throughout the rings (Etxaluze, M. et al. 2014). These molecules form through low energy collisions in dense environments, which makes the collisions more likely and protects the bonds from breaking by shielding from UV radiation. This all requires neutral atomic carbon to bond with other atoms or smaller molecules to form more complex molecules such as CO, HCO^+, HCN, and HNC. [C I] also serves to shield the inner regions of the PDR from the harsh UV radiation.

In this study, the $^3P_1 \rightarrow ^3 P_0$ transition (492 GHz) of [C I] has been measured. In PDR chemistry, this atom is most prevalent at temperatures slightly higher than those found inside of the globules, at 25 K (Bachiller et al. 1997). At temperatures significantly higher and lower than this, the abundance of [C I] significantly decreases as it is ionized at higher temperatures and is much more likely to form molecular bonds at lower temperatures. By examining the structure of [C I] in more detail than before, we will be able to more clearly understand the role that [C I] plays in the PDR in this oxygen-rich planetary nebula. These results will also further our understanding of how the outer layers of this former low mass star are being recycled into the Interstellar Medium (ISM).

We now present the highest resolution maps of [C I] to date at 0.49″ using the Atacama Compact Array (ACA). In section 2 we describe the observation and data reduction details. Section 3 examines the spectra of [C I] at the three observed positions and shows calculations of upper limits for the transitions that were not resolved. Section 3 also gives a comparison of the [C I] spectra with the molecular spectra from the IRAM-30m telescope (Bublitz et al.

2022). In Section 4 we show the maps of [C I] at the two regions where detections were resolved and examine the structure at different velocities. In Section 5, we compare the ACA [C I] maps with HST images of [O III] and Hα (Meixner et al. 2005).

2. OBSERVATIONS

In the accepted proposal, observations were supposed to be taken for the [C I] and HC_3N lines at six positions across the Helix Nebula. The velocity resolution was 0.344 km s^{-1} for the [C I] line and 0.345 km s^{-1} with a spatial resolution of 0.49 arcseconds. The six positions were divided between two regions in the outermost layers, referred to as the East and West positions, three globules, Globules A, B, and C, and one transitionary position, referred to as the Rim position (see Figure 1). Globules are regions of dense molecular gas closer to the CSPN inside of the ionized cavity that are being irradiated. They are a prime example of a photodissociation region (PDR), where the main chemistry is being driven by the UV-radiation coming from the CSPN. They extend radially from the CSPN, with many featuring slightly more diffuse tails behind the denser heads (Bublitz, Steffes, et al, 2022, in prep). All of these are behind dense regions of ionized gas (Meixner et al. 2005) and are being driven outwards as the former low mass star returns its outer layers to the ISM and becomes a white dwarf star.

Data inspection and reduction were performed with CASA (Common Astronomy Software Applications), a software package by NRAO that flags problems in data and does primary data processing and imaging for data taken using the Atacama Large Millimeter Array (ALMA) and the Very Large Array (VLA), among other radio telescopes. Originally, this data was intended to be collected for a total of 40 minutes of integration time on each of the six sources (Figure 1). However, because ALMA was shut down for several months due to the COVID-19 Pandemic, time constraints meant that none of the observations at Globules A, B, or C were taken. Much of the integration time on East and West Positions were also lost. These positions received 50% and 32% of their requested integration times, respectively. Only the Rim position was observed for the full integration time.

As the East and West positions had not received their full integration time, they had also not been run through the ALMA pipeline to be calibrated, so this was done. While conducting the data reduction, no flagging was applied before the continuum subtraction. Based on the frequency, it was determined that each of the files should have dimensions of 72x72 pixels. The approximate velocities of any likely detections were determined based on the velocities of molecular emission lines in Bublitz et al. (2022). 30 km s^{-1} were added to either side of the molecular detection to be sure that the entire profile was captured. The proposed velocity resolutions were used when performing the TCLEAN. Individual channels are then examined and a mask is drawn around the regions where a signal is observed. This is then run through iterations until the signal blends in with the noise and each subsequent iteration yields no change. This mask is then subtracted to most effectively only remove noise and improve the signal-to-noise ratio (SNR).

3. SPECTRA

Examining the spectra for the entire region of the Rim, East, and West positions, the difference in integration time is apparent (Figures 2, 3). The SNR is greatest at the Rim position at approximately 13, which had the longest integration time, and lowest for the West position 1, with the shortest integration time. The East position had a SNR of 3.2. Analysis of the Rim position spectra indicates two components of [C I] detected (Figure 2, left). The higher intensity detection peaks at a velocity of –47.3 km s^{-1} being blue-shifted from the systemic velocity of –23 km s^{-1} (Figure 2, left). The peak for the blue-shifted velocity is at a maximum of 1149.26 Jy. The lower intensity detection of [C I] peaks at a red-shifted velocity of –9.8 km s^{-1}. The red-shifted component has a maximum intensity of 221.54 Jy. The spectrum at the East position peaks at a maximum intensity of 148.35 Jy at a velocity of –29.5 km s^{-1}, being slightly blue-shifted from the systemic velocity (Figure 2).

3.1. *Comparison with IRAM 30m Data*

The spectra showing the [C I] data collected using the ACA was then compared with the molecular lines collected with the Institut de Radioastronomie Millimétrique (IRAM) 30m single dish telescope (Bublitz et al. 2022). HCO^+ was selected for spectral comparison due to its strong signal.

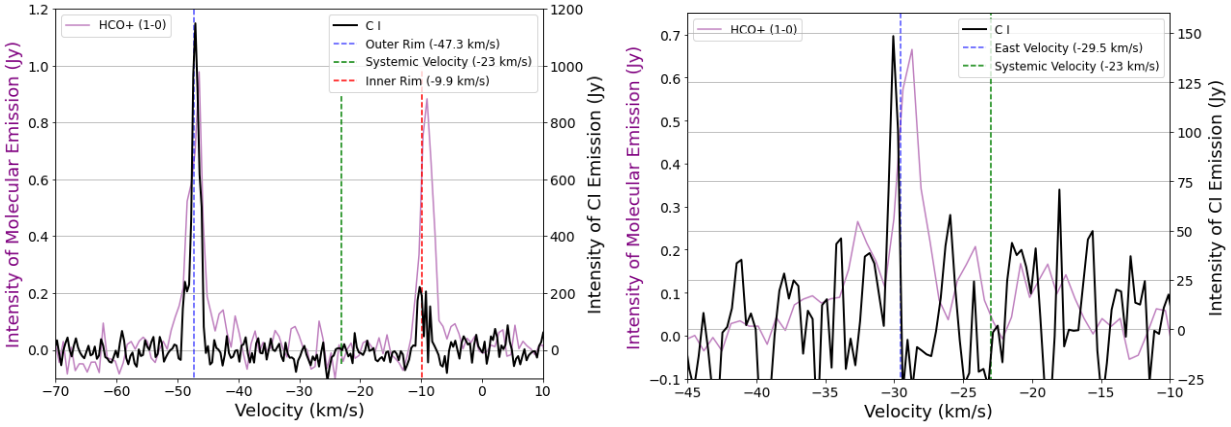

Figure 2. Spectra of [C I] (black) and HCO^+ (purple) at the Rim (left) and East (right) positions. The systemic velocity (green) and bulk gas velocities (blue and red, Bublitz et al. 2022) are noted with vertical lines.

At the Rim position, the peaks in HCO^+ line up well with those in [C I]. There is a small offset between the data sets less than a channel wide, which can be attributed to differences in velocity resolution between data (Figure 2, left). However, while the HCO^+ line peaks to nearly the same intensity at both velocities (∼1 and ∼0.9 Jy at the blue- and red-shifted velocities respectively), this is not the case in [C I], where the intensity at the blue–shifted velocity is approximately six times that of the intensity at the red–shifted velocity. In the [C I] spectra the blue- and red-shifted velocities have respective maximum intensities of ∼1150 and ∼200 Jy. While there could be nearly six times as much [C I] present at the Outer

Rim position as compared to the Inner Rim, another possibility is that the blue-shifted gas is partially absorbing the [C I] emission from the red-shifted gas, which does not occur in the molecular transitions. Currently, there is insufficient information to conclude a cause for this phenomenon. Additional analysis and modeling is required to ascertain the cause of asymmetrical emission in [C I]. Observations of the region in infrared or full maps of molecular lines may also provide a more detailed explanation.

The spectrum for the East position shows a much lower SNR than the Rim position (Figure 2). However, there is still a clear detection of [C I] at approximately –31 km s^{-1}. Comparing with the HCO^+ data from the IRAM 30m telescope, reveals a slight offset in the peak velocities. While a similar, albeit smaller offset was also detected at the Rim, the peak at the East position is offset by a difference of over 1 km s^{-1}. Though the cause of this offset remains unclear, the entirety of the [C I] detection does still fall within the wings of the HCO^+ emission and thus is representative of the same region of emitting gas.

3.2. *Upper Limit Calculations*

3.2.1. *Neutral Carbon in the West Position*

While [C I] was not detected at the West position due to the low integration time, previous maps have shown the region to be abundant in [C I] (Young et al. 1997). Based on the IRAM 30m low–intensity molecular features and past publication of lower resolution maps (Bublitz et al. 2022; Etxaluze, M. et al. 2014), it is reasonable to anticipate the West position also has a low intensity signal, which remains hidden in the noise. An overlay of HCO^+ from Bublitz et al. (2022) shows three features- at velocities of approximately -29.5, -20.5, and -10.5 km s^{-1}, indicative of the general structure of gas expected in the [C I] data. Further integration towards this position is required to confirm. The lack of a clear detection also made it impossible to map [C I] in this region.

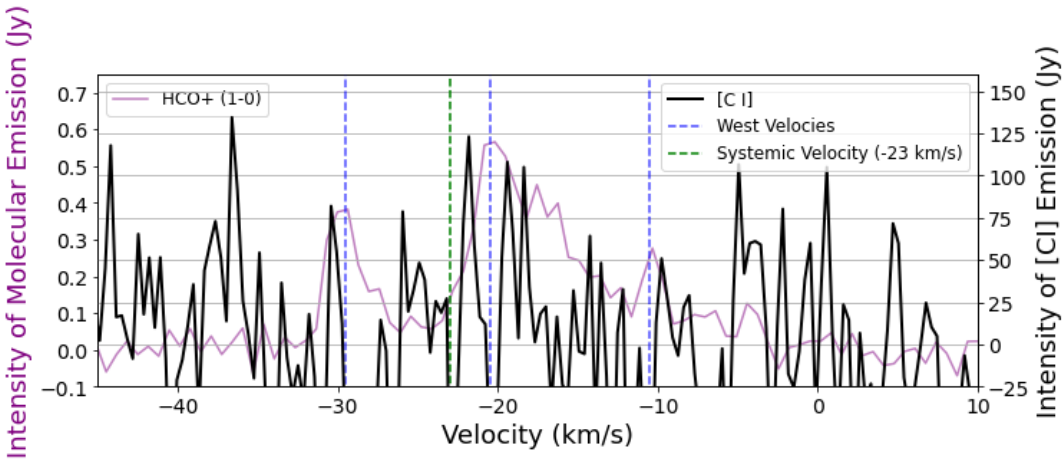

Figure 3. The purple spectrum shows that of HCO^+ with the velocities of peak intensity being indicated in blue vertical lines (Bublitz et al. 2022)

The levels of HCO^+ and the previous detection of [C I] around the West position, indicate that there should be [C I] in the region. To estimate the upper limits of [C I] in the West position, we calculate the Root Mean Squared (RMS) of the spectrum at the range of velocities where we expect to find a detection. In this case, due to the broad emission features of HCO^+, we calculate the RMS of the entire range from -32.8 km s^{-1} to -8.7 km s^{-1}. This yields an upper limit of [C I] emission of 66.4 Jy. Given the noise levels dramatically exceeding this estimation, reaching a level of approximately 125 Jy, it is clear why a detection of [C I] was not resolved.

3.2.2. *HC_3N in the East, West, and Rim Positions*

No HC_3N was detected in the three positions observed. However, given the abundance of other molecular species detected in the regions (Bublitz et al. 2022), HC_3N may exist in the extended Helix envelope. Being a more complex molecule, HC_3N is found in the denser regions of PDRs where other smaller molecules, such as HCN and HNC, are found in higher quantities. These regions have a higher amount of shielding from UV radiation coming from the CSPN. HC_3N is observed in Globules B and C, which are closer to the CSPN and offer denser environments than those observed here (Bublitz, Steffes, et al, 2022, in prep). However, in the globules, HC_3N is observed at lower intensities than many of the other molecular transitions and is restricted to only the densest parts of the globules. Although HC_3N was not detected in the East, West, or Rim positions, upper limits for this molecular transition have been computed (Table 1).

Table 1. Upper Limits of HC_3N

Position	Velocity Range (km s^{-1})	Upper Limits (Jy)
Outer Rim	-50.01 – -44.83	53.37
Inner Rim	-11.34 – -6.85	40.17
East	-32.77 – -8.61	78.19
West	-33.46 – -26.56	37.39

The upper limits of HC_3N were calculated by taking the RMS over the ranges of velocities in which HC_3N was expected to be found. These regions were based on the velocities of detections of [C I] and molecular species, as indicated by the spectra in Figure 4 (Bublitz et al. 2022). As the Rim position shows two different features at the separate velocities, the upper limits of HC_3N were calculated for both- one at the red-shifted velocity (the Inner Rim) and one at the blue-shifted region (the Outer Rim). The West position had a much broader velocity range due to the multiple broad peaks found in the molecular transitions, so the upper limits of [C I] were calculated using the RMS for this entire range (Bublitz et al. 2022).

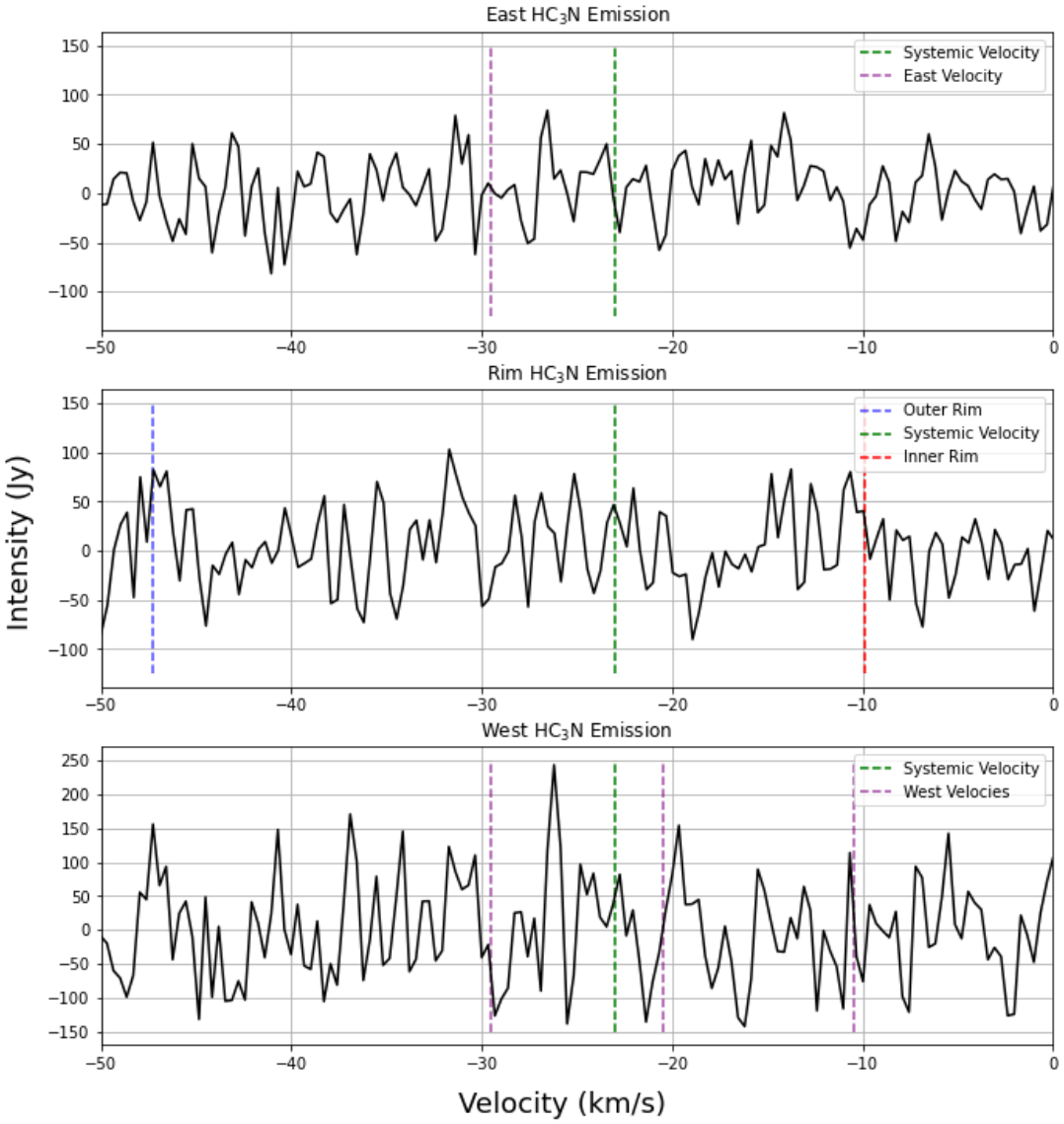

Figure 4. The HC_3N spectra at the East (top), Rim (center), and West (bottom) positions. The systemic velocities are indicated in green with the velocities of peak intensity of HCO^+ being indicated in red, blue, and purple (Bublitz et al. 2022).

4. MAPPING OF NEUTRAL CARBON

Moment 0 maps were created for the two regions with clear detections of [C I], the Rim and East positions. This was done to examine the structure of the regions and, at the Rim position, examine how it varied between the two velocities (Figure 5). Due to the relatively low SNR and that the detections of [C I] were rather narrow, the only velocity channels included in the Moment 0 maps were the channels that included any structure based on a visual investigation of individual channel maps. Moment 0 maps are created using the following equation: $\int I_\nu \, d\nu$, which sums the intensity along each of the velocity channels and multiplies by the velocity resolution of [C I] (0.344 km s^{-1}).

4.1. *Moment 0 Maps*

The Moment 0 map for the Rim position includes two subsections in the summation, made up by the two features seen in the spectrum (Figure 5, left). In the case of the Rim position, the higher intensity blue–shifted region spanned 10 channels, making the detection approximately 3.44 km s^{-1} wide. The lower intensity red–shifted region was slightly wider, spanning 11 channels at a width of 3.78 km s^{-1}. This region has a total integrated intensity of 2205.8 Jy km s^{-1} and a maximum integrated intensity of 5.41 Jy beam^{-1} km s^{-1}. The main structure is found in the center of the region, extending radially away from the CSPN (Figure 5, left). The shape of this main structure at the Rim position follows what can be expected from a globule-like structure in that it has a long tail and the shape is driven by UV-radiation (Andriantsaralaza et al. 2019). The regions of maximum integrated intensity are found along the edges of the observations, which could be the product of edge effects and are examined in further detail in Section 5 (Figure 5, left).

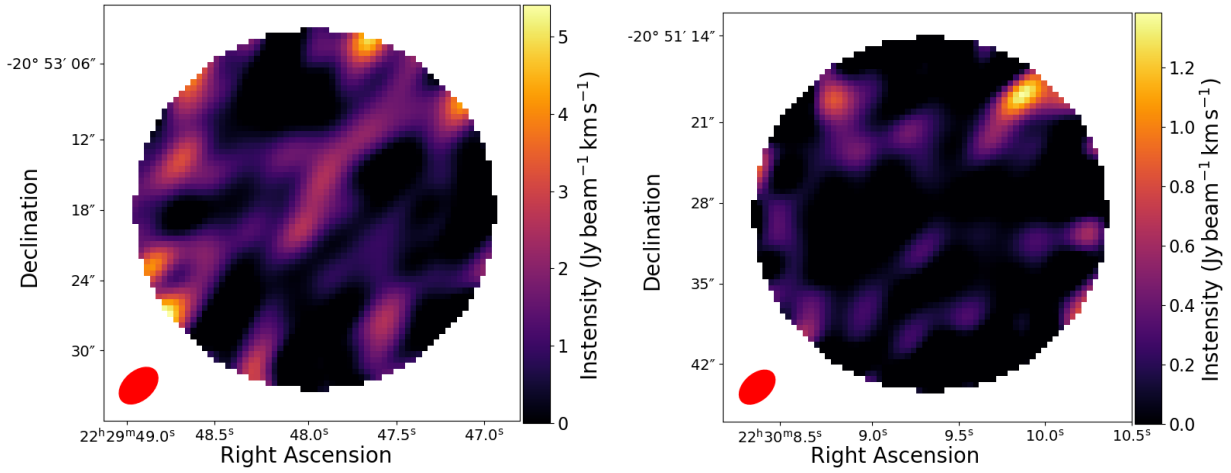

Figure 5. Moment 0 Maps of [C I] at the Rim (left) and East (right) positions. The beam size is indicated in the bottom left corners.

In contrast to the Rim position, the East position spectrum only had a single prominent feature, spanning 7 channels for a width of 2.41 km s^{-1} (Figure 2, right). The entirety of the detection is blue–shifted with respect to the systemic velocity. The detection of [C I] at the East position has a total integrated intensity of 99.20 Jy beam^{-1} km s^{-1} and a maximum integrated intensity of 1.39 Jy beam^{-1} km s^{-1}. One main component can be seen in the north-western edge of the map. This larger and brighter clump is also the location of the highest integrated intensity line. Unlike the Rim position, none of the clumpy regions of [C I] extend radially from the CSPN. Rather, each are scattered about the region with no discernible direction (Figure 5, right).

4.2. *Mapping the Multiple Velocity Components of [C I]*

In both the East and Rim positions, contours showing the progression of velocities were added on top of the Moment 0 maps to more clearly illustrate the three-dimensional structure

of the gas in these regions. At the Rim position, red and blue contours were used to trace the outside of the gas within a 2σ significance. The blue–shifted gas makes up the globule-like larger structure along with some smaller clumpy pieces. The red contours do not outline many of the main structural elements the way that the blue contours do. This matches the spectra in Figure 2, as the red-shifted gas had a much lower intensity than the blue–shifted counterpart. This map could support the hypothesis that some of the emission from the red-shifted feature is being absorbed by the globule-like structure at the blue shifted position, obscuring any structural elements at the red–shifted position. There is almost no red–shifted gas seen towards the middle of the map, with any red shifted gas being outlined nearer to the edges, where there is a decrease in blue–shifted gas.

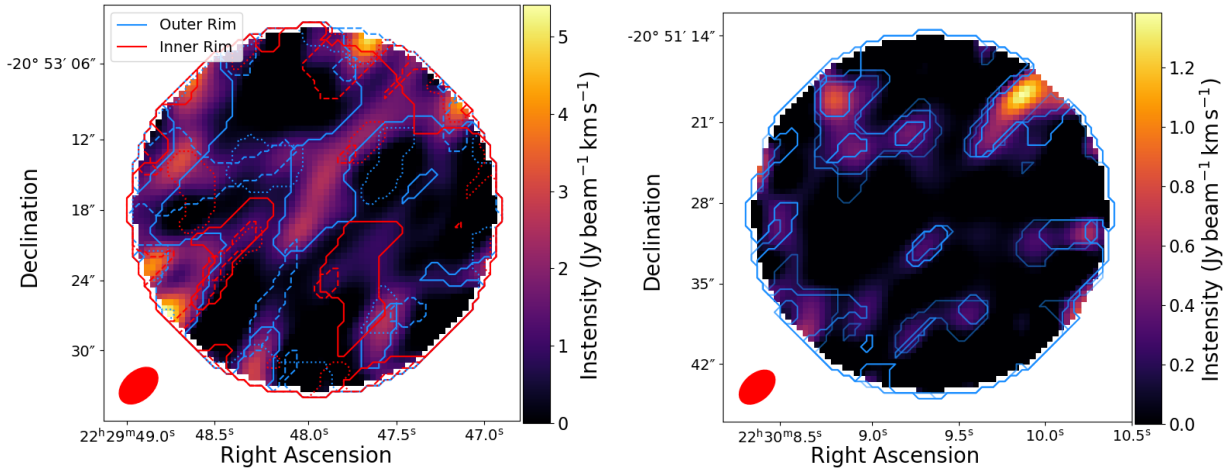

Figure 6. Moment 0 Maps at the Rim (left) and East (right) positions with contours of 2-3 consecutive velocity channels. The beam size is shown in the bottom left.

Because the [C I] gas at the East position was only detected at one velocity range, the contours are only shown in blue. Each outlines two consecutive velocity channels, spanning the entire width of the detection within a 2σ significance. This illustrates the three-dimensional structure and confirms that the smaller, lower intensity clumpy parts were more than convenient noise. As each of the regions do span a minimum of four velocity channels, with at least two contours, it further shows that the [C I] in the East position is comprised of small, low intensity PDRs, rather than the spatially expansive diffuse gas, as was previously assumed.

5. COMPARING [C I] MAPS WITH OPTICAL DATA MAPS FROM HST

5.1. *Zooming in and Cropping Hubble Space Telescope Images*

An important aspect to this analysis was the comparison of [C I] to [O III] and Hα from the Hubble Space Telescope (HST) (Meixner et al. 2005). The HST collected data from across nearly the entire Helix Nebula, though not the diffuse outer envelope that contains the East and West positions. The position with the highest signal to noise ratio, the Rim

position, was available in the HST image. Because the ACA examined very small regions (0.009664 degrees in diameter) compared to the entire HST Helix Nebula image (0.26 degrees in diameter) only a small region of the HST images was required.

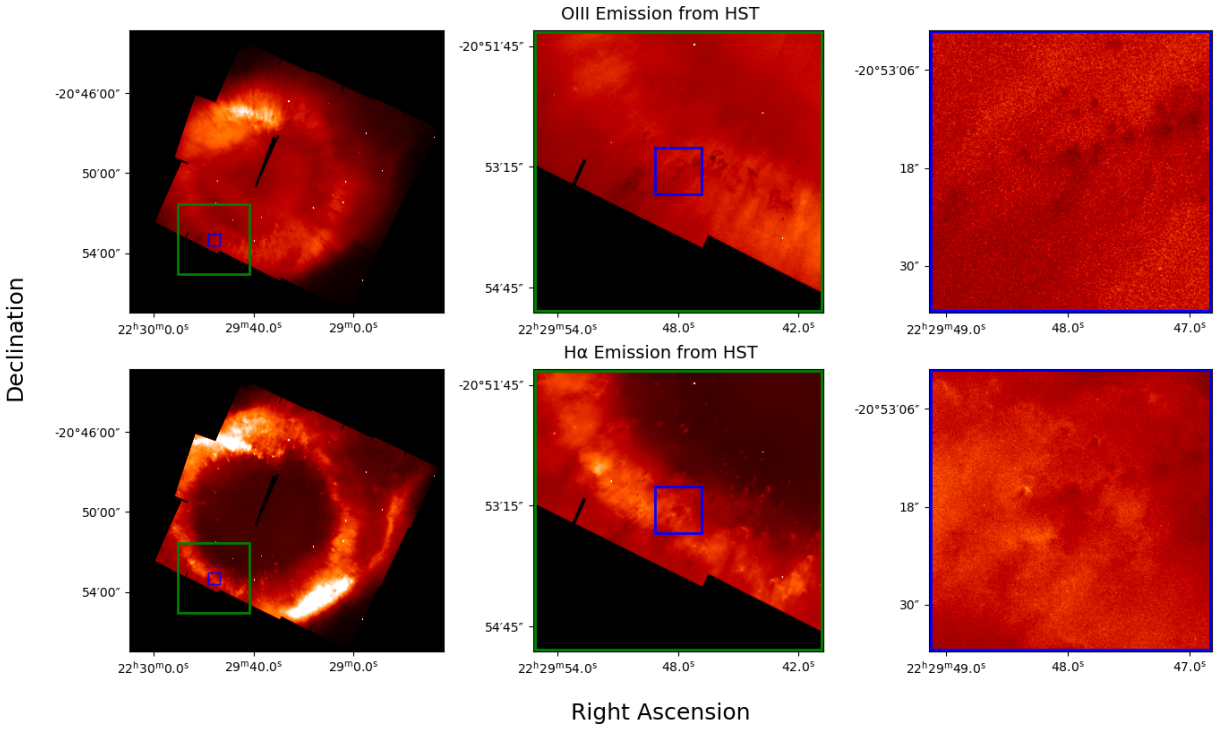

Figure 7. HST observations of [O III] (top) and Hα (bottom) (Meixner et al. 2005) at different scales. Colored squares represent the sequence of zoomed in images towards the Helix Rim position observed in this work.

To crop and zoom in on the proper region, the HST data was first rotated counterclockwise by 64.7737° to correct the orientation of the image. This rotation changes the dimensions of the image, so the right ascension and declination were redefined based on a new known reference point (Figure 7, left). Intermediate images were also made while cropping to view the entire region and compare with what was seen while viewing the maps on SAO DS9 (Figure 7, center). The final images match the size of the maps from the ACA in [C I] though map the region in [O III] and Hα (Figure 7, right). These zoomed in maps of the HST data compare the ionized and higher energy transitions to the low energy transitions of neutral carbon that were detected in Section 5.

5.2. *Overlaying [C I] contours on HST maps*

The contour maps showing [C I] at the Rim position were then overlaid onto the maps of Hα and [O III] from HST. An inverted colorbar was used to highlight the regions where there was a lack of Hα or [O III] emission (Figure 8). In both cases, the contours from both the red– and blue–shifted gas lines up well with where there is a decrease in emission from the higher energy transitions. This follows the PDR model, in that the ionized gas surrounds

the colder denser regions of atomic and molecular gas. The atomic gas is also expected to surround the even denser molecular gas, though still be interspersed throughout the cloud, as is expected to be occurring here.

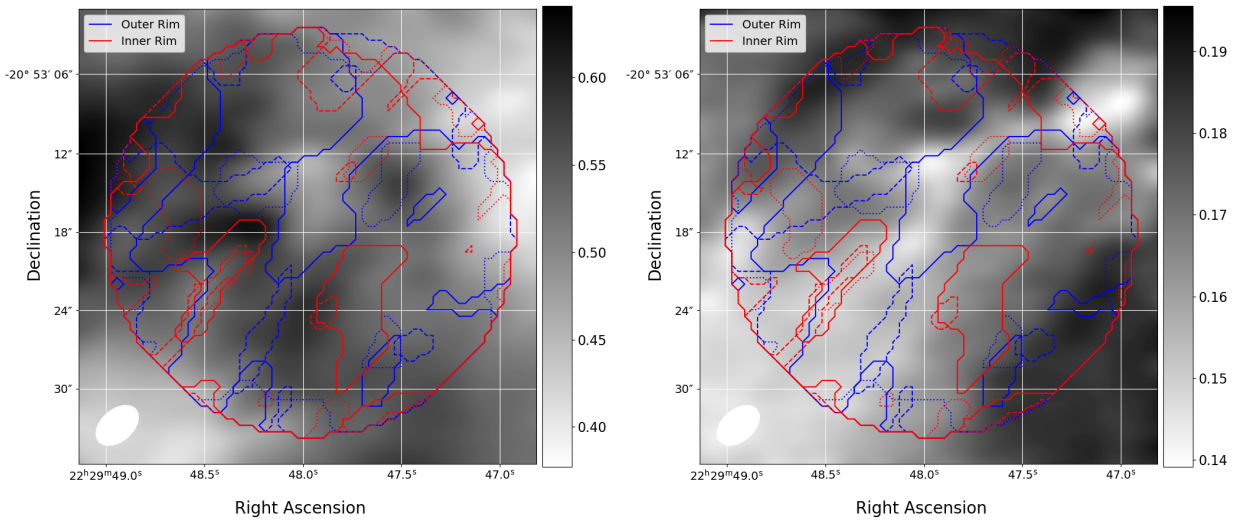

Figure 8. Maps of Hα and [O III] from HST (Meixner et al. 2005) at the Rim position with [C I] contours overlaid on top. The ACA beam size is indicated in the bottom left corner.

The higher energy transitions both show the gas extending radially away from the CSPN, lining up with the main globule-like feature at the blue–shifted velocity. Not much other structure can be seen that does not directly align with what is seen in [C I] (Figure 8. This could suggest further evidence to refute the possibility of the blue–shifted globule–like structure absorbing some of the emission from the red–shifted component. However, as with this entire body of work, more analysis would be required to draw more concrete conclusions about either hypothesis.

6. CONCLUSIONS

This is the highest resolution mapping of [C I] in the Helix Nebula, which was created using the Atacama Compact Array. Maps were created at the East and Rim positions, as the other four intended positions were not mapped due to the data not being observed or observed for too short of an integration time to detect [C I]. In the two regions where [C I] was detected, comparisons were made using Moment 0 maps and the spectra compared with molecular data collected by the IRAM-30m telescope (Bublitz et al. 2022). The comparisons with the HCO^+ spectra lined up well with the [C I] spectra and suggest two components at the Rim position- one red–shifted and one blue–shifted. However, the difference in intensities between the red– and blue–shifted regions suggests the possibility of an absorption feature, that requires further observation to draw any conclusions. Mapping the Rim position shows globule–like structures at the Rim position, a region which was previously obscured by dust. The map at the East position shows a number of small, low intensity clumps of [C I], which span several velocity channels, rather than the previously assumed low intensity expansive

gas across the region. The molecular gas detected in this region by the IRAM-30m telescope is likely in these isolated clumps, which follows the PDR model.

ACKNOWLEDGEMENTS

This paper makes use of the following ALMA data: ADS/JAO.ALMA#2019.2.00039.S. ALMA is a partnership of ESO (representing its member states), NSF (USA) and NINS (Japan), together with NRC (Canada), MOST and ASIAA (Taiwan), and KASI (Republic of Korea), in cooperation with the Republic of Chile. The Joint ALMA Observatory is operated by ESO, AUI/NRAO and NAOJ. The National Radio Astronomy Observatory is a facility of the National Science Foundation operated under cooperative agreement by Associated Universities, Inc.

The authors would also like to thank the Green Bank Observatory and NRAO REU program, funded by the National Science Foundation, which provided the opportunity for this project. A huge thank you is also extended to the other 2022 Summer Students and Mentors at the Green Bank Observatory for their continual support.

REFERENCES

Andriantsaralaza, M., Zijlstra, A. A., & Avison, A. 2019, Monthly Notices of the Royal Astronomical Society, 491, 758

Bachiller, R., Forveille, T., Huggins, P., & Cox, P. 1997, Astronomy & Astrophysics, 324, 1123

Bublitz, J., Kastner, J. H., Hily-Blant, P., et al. 2022, Astronomy & Astrophysics, 625, A101

Etxaluze, M., Cernicharo, J., Goicoechea, J. R., et al. 2014, A&A, 566, A78

Gaia Collaboration, Brown, A. G. A., Vallenari, A., et al. 2018, A&A, 616, A1

Meixner, M., McCullough, P., Hartman, J., Son, M., & Speck, A. 2005, The Astrophysical Journal, 130, 1784

Young, K., Cox, P., Huggins, P. J., Forveille, T., & Bachiller, R. 1997, The Astrophysical Journal, 482, L101